Learning Displacement Signals Directly from the Wrapped Interferograms Using Sentinel-1 and Artificial Intelligence

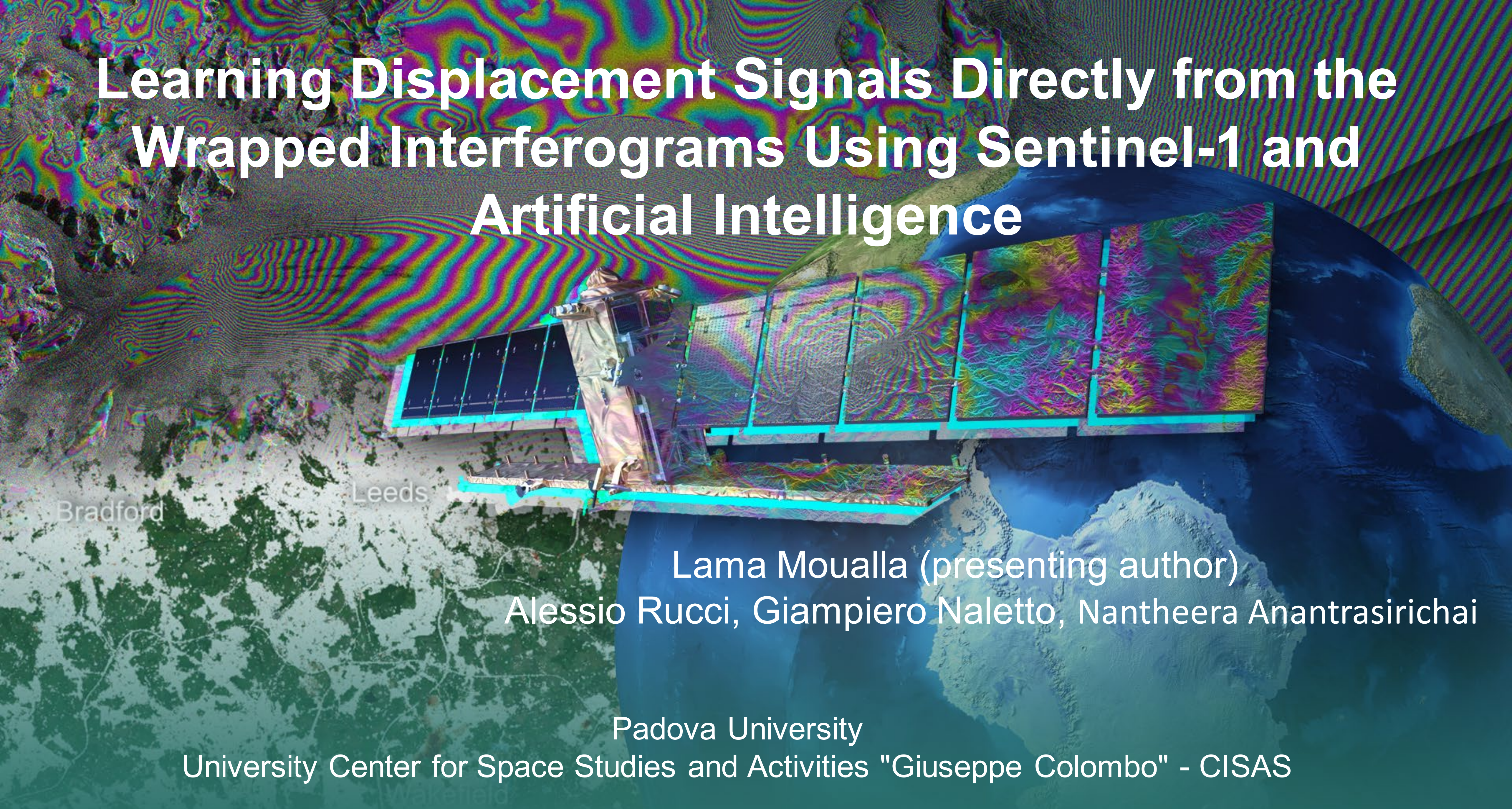

Lama Moualla (presenting author)
Alessio Rucci, Giampiero Naletto, Nantheera Anantrasirichai

Padova University
University Center for Space Studies and Activities "Giuseppe Colombo" - CISAS

Table of Contents

Challenges in Deploying InSAR Technology

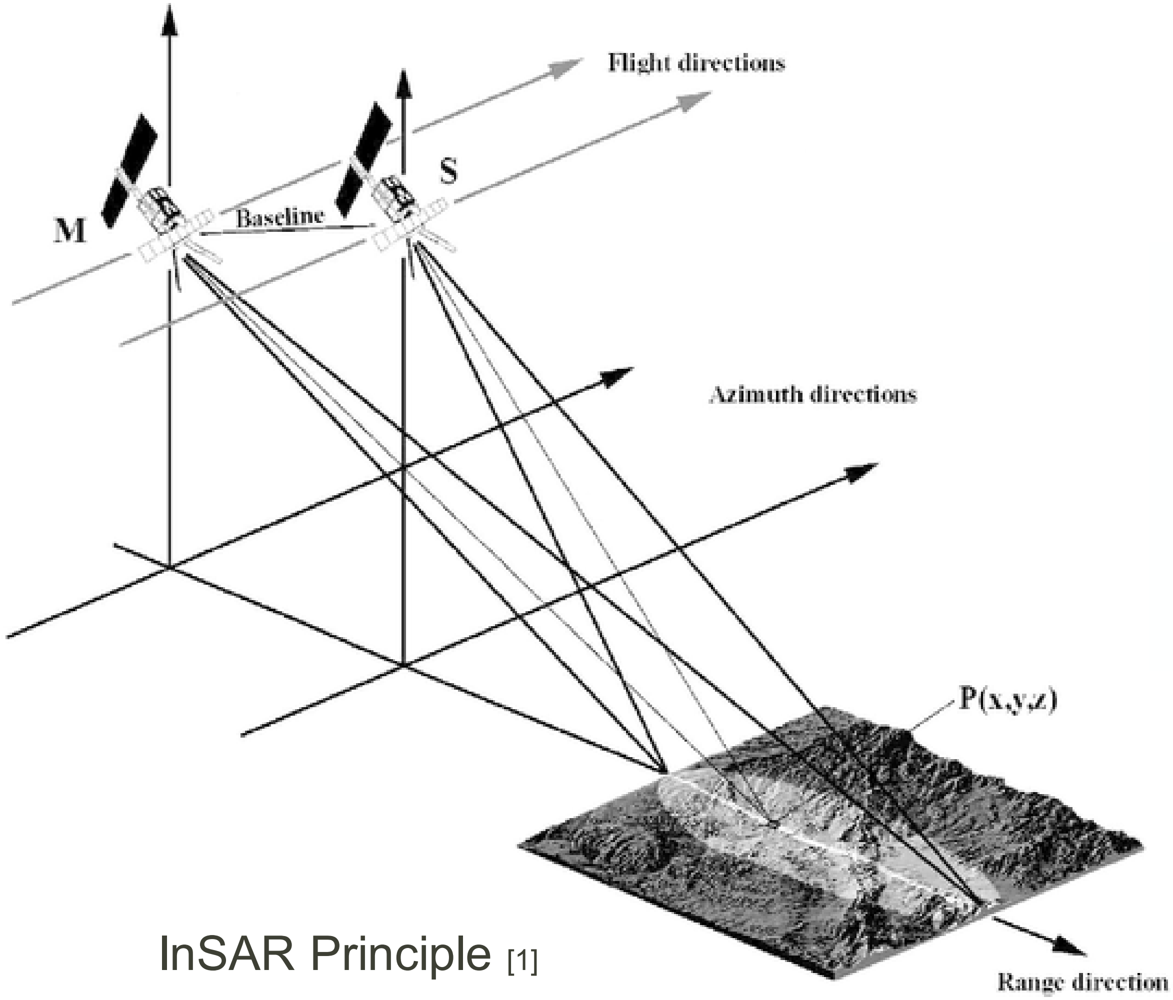

InSAR Principle [1]

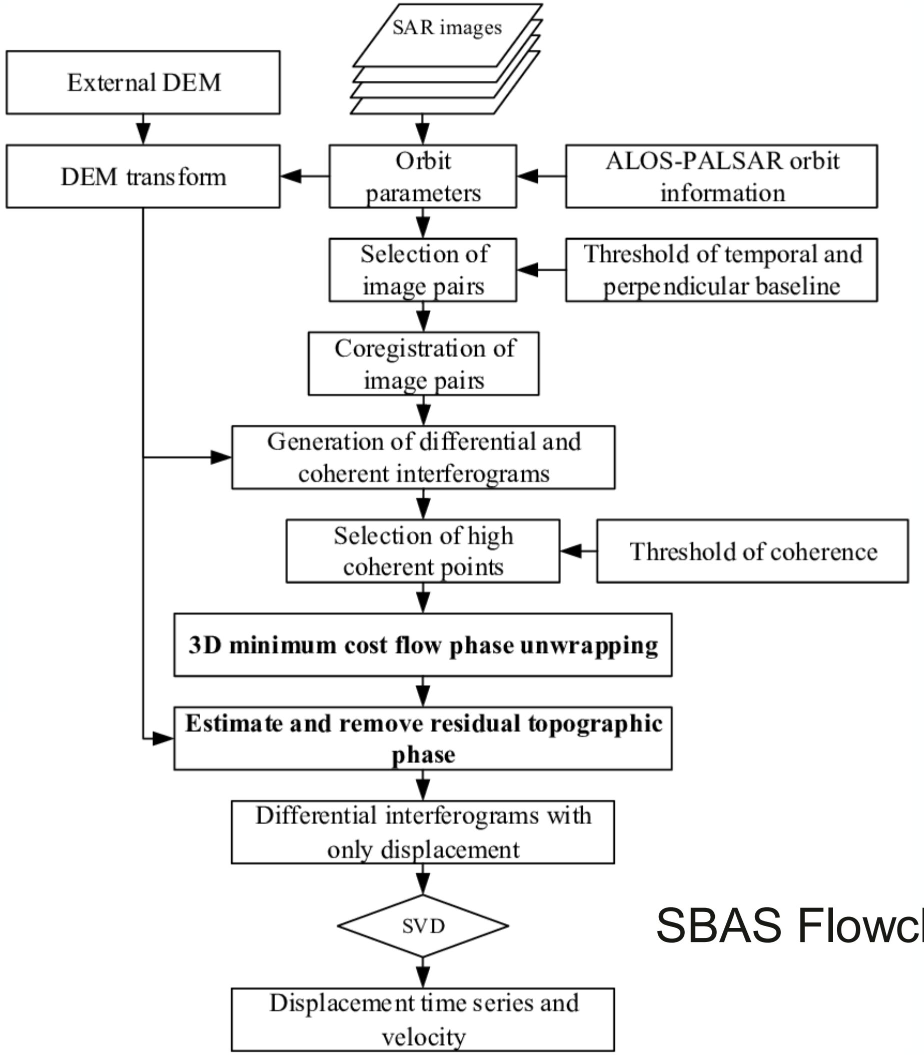

SBAS Flowchart [2]

Challenges in Deploying InSAR Technology

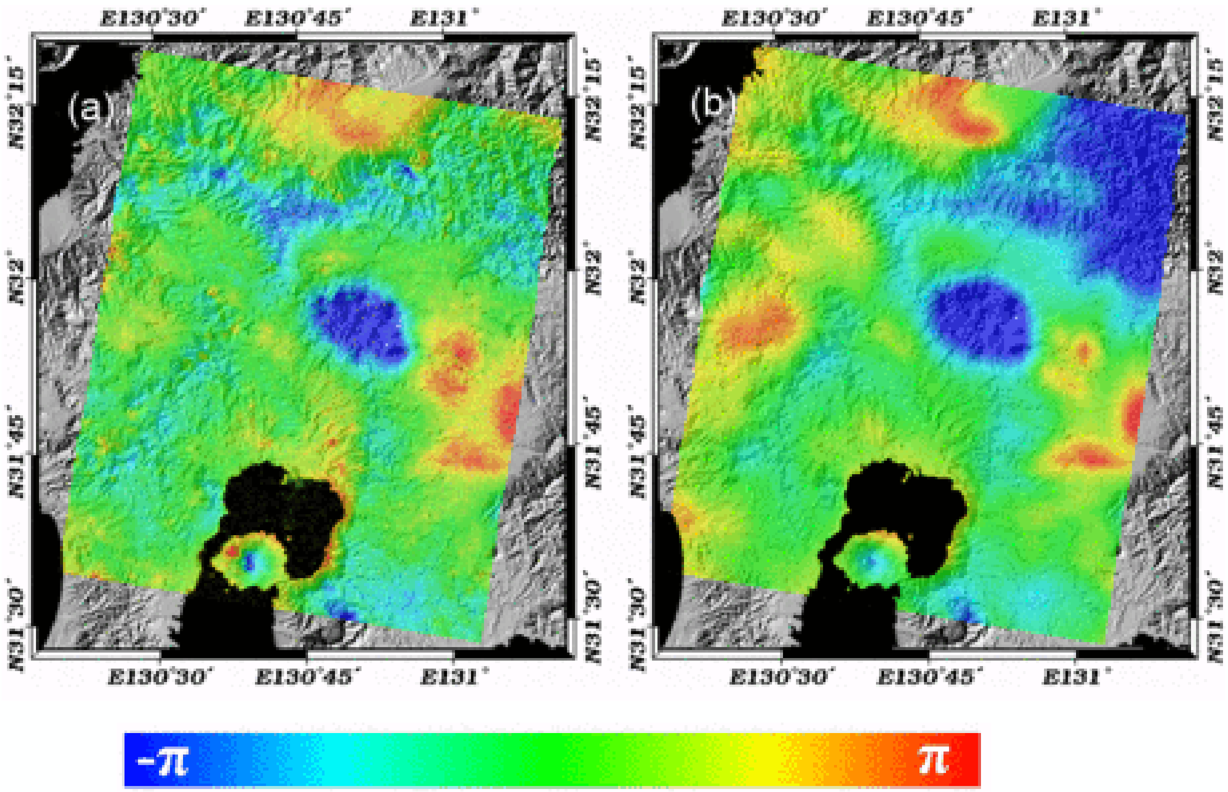

Atmospheric Phase Screen [3]

How to mitigate the distortions in the radar signal's phase as it passes through the Earth's atmosphere affecting the accuracy of displacements measurements?

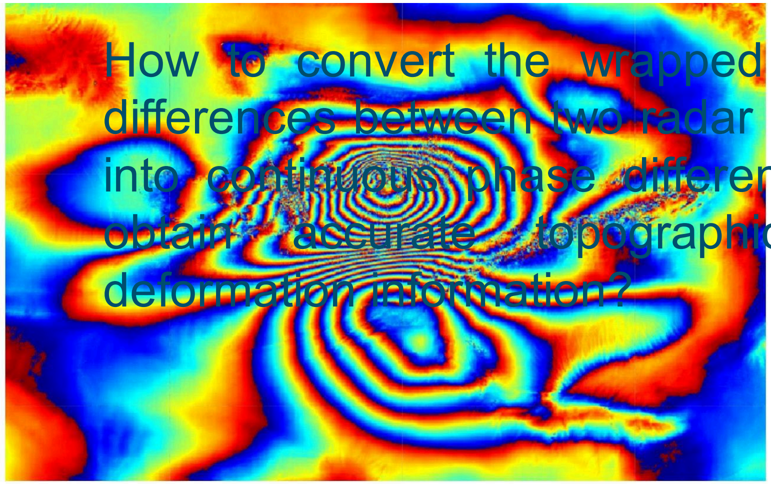

How to convert the wrapped phase differences between two radar images into continuous phase differences to obtain accurate topographical or deformation information?

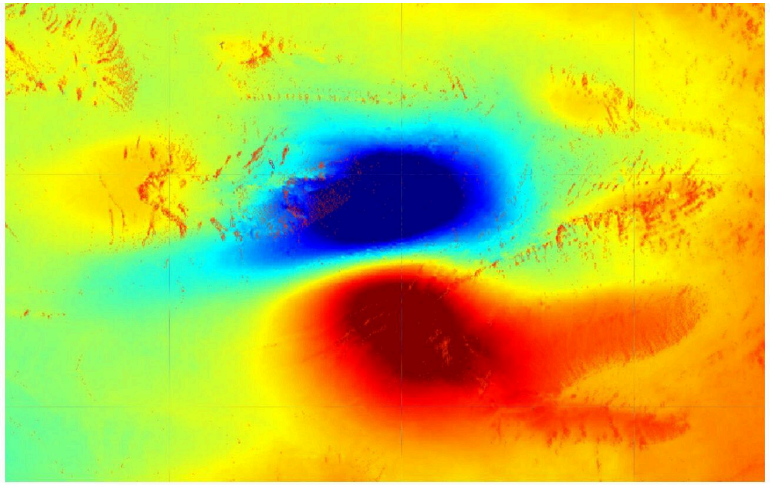

Phase Unwrapping

Challenges in Deploying InSAR Technology

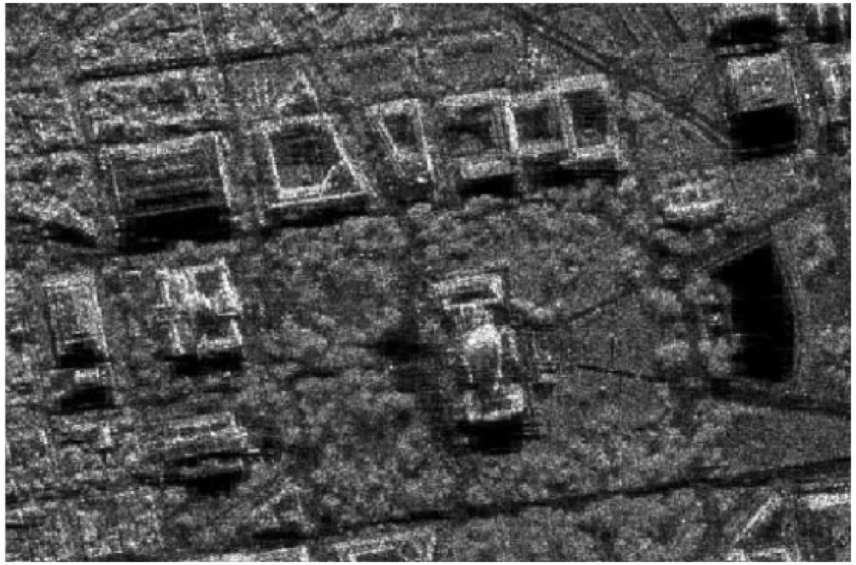

What are the geometric factors between the radar sensor and the terrain or structures being imaged:
- The angle of incidence of the radar beam?
- The orientation of the terrain features?
- The altitude and position of the radar platform?

Speckle Noise [4]

How to filter the noise resulting from coherent interference of scattered radar signals?

Geometric Distortions [5]

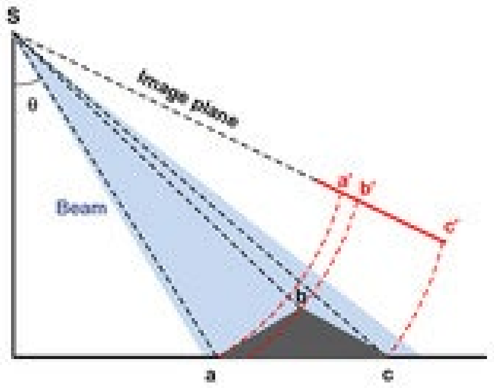

Foreshortening

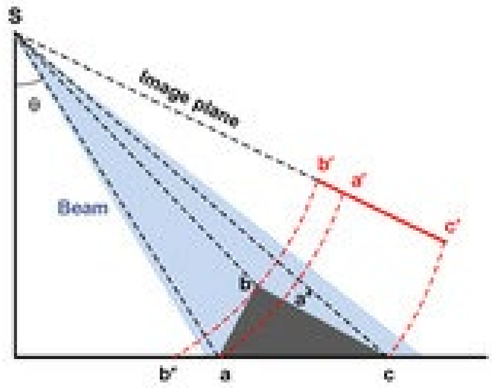

Layover

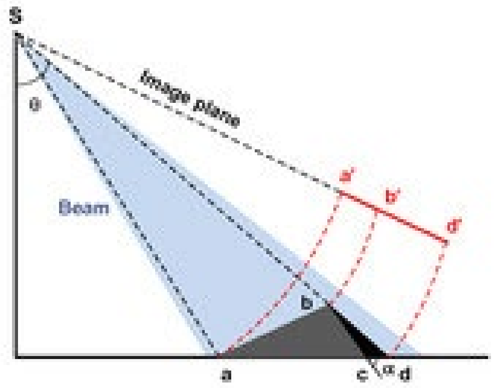

Shadowing

The Main Objective

Employing Intelligent algorithms in developing a methodology that can automatically analyze large InSar data sets. This methodology is formulated to delineate regions where infrastructures are susceptible to displacements induced by terrestrial movements. Notably, this approach circumvents the need for more intricate multi-temporal InSAR analyses, such as phase unwrapping. Instead, it leverages only the wrapped interferograms and coherence maps as its input parameters for identifying areas of motion.

By: NoR esa

Sponsorship

Cloud computing environments make available a large collection of computing resources and storage that can be effectively exploited through the presented S1 P-SBAS processing chain to carry out interferometric analyses at very large scales in reduced time frames

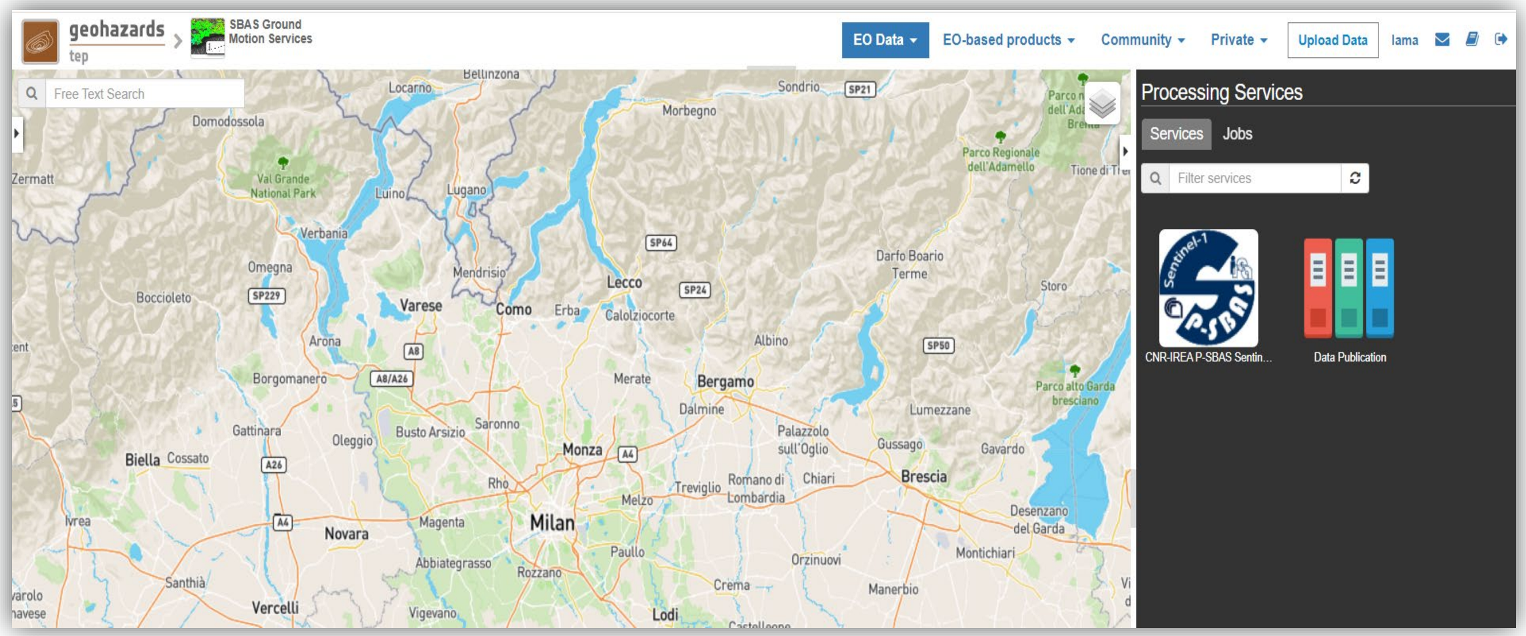

Parallel - Small BAseline Subset (Lombardy - Italy)

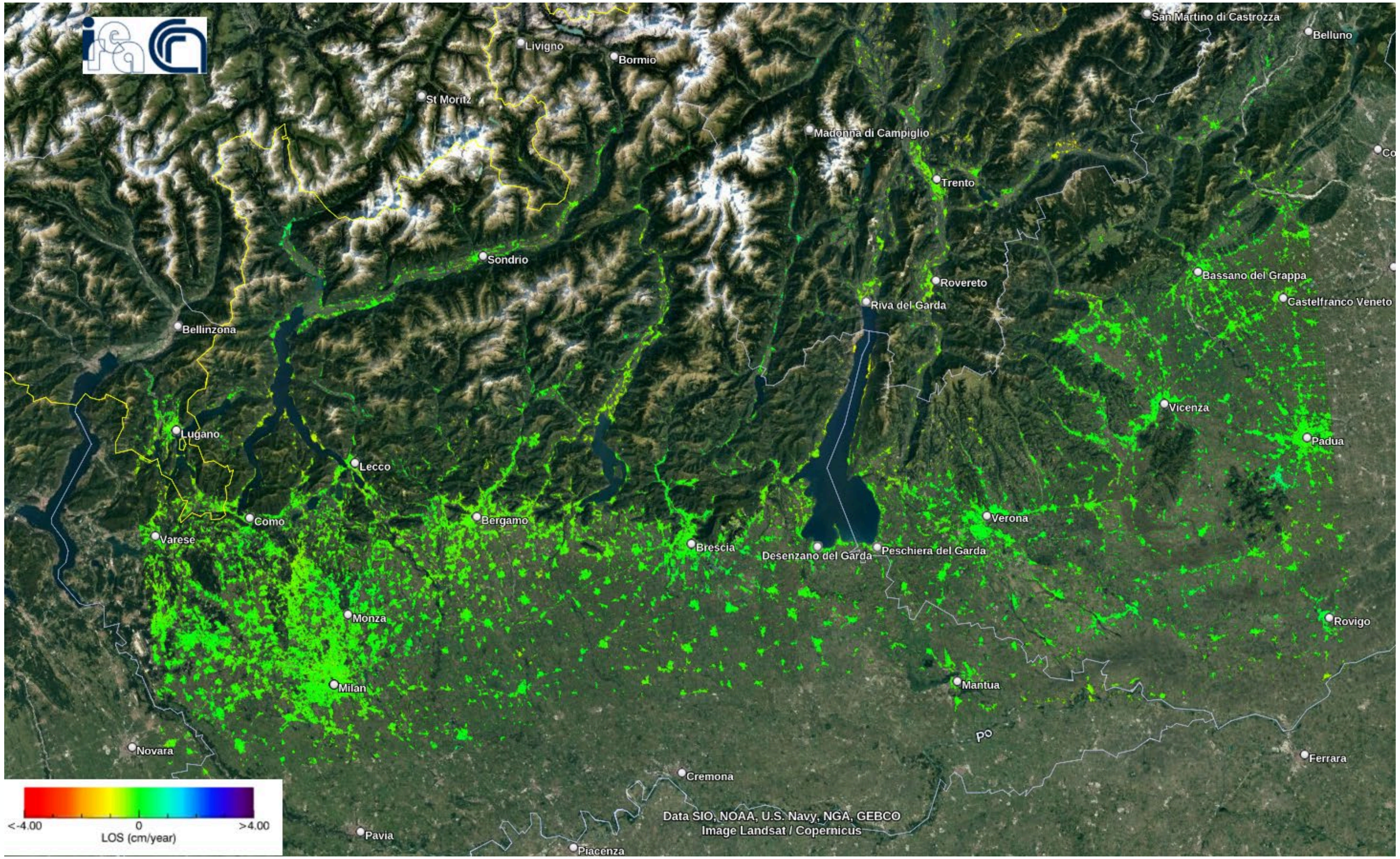

Start Date	07/01/2020
End Date	17/08/2021
Number of Images	50
DEM	SRTM1 arcsec
Temporal Coherence	0.85
Bounding Box	44.943 , 8.693 46.884 , 12.231
Orbit Direction	Descending

The selected parameters using the P-SBAS service at G-TEP platform to create Lombardy deformation velocity map, the interferograms and the coherece map.

Parallel - Small BAseline Subset (Washington - USA)

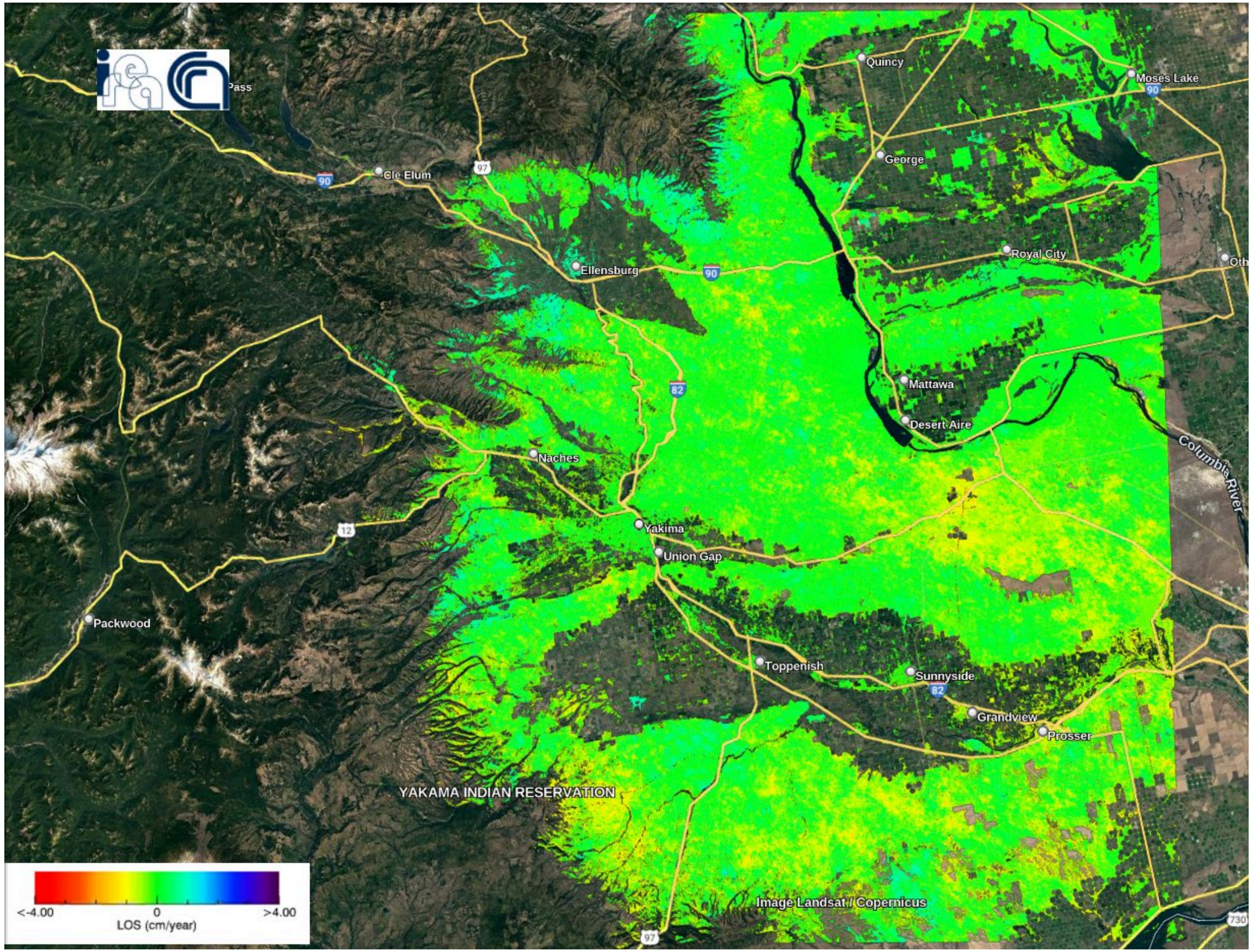

Start Date	14/10/2016
End Date	28/12/2019
Number of Images	75
DEM	SRTM1 arcsec
Temporal Coherence	0.7
Bounding Box	-121.426 , 46.358 -120.042 , 47.167
Orbit Direction	Ascending

The selected parameters using the P-SBAS service at G-TEP platform to create Washington deformation velocity map, the interferograms and the coherece map.

Parallel - Small BAseline Subset (Lisbon - Portugal)

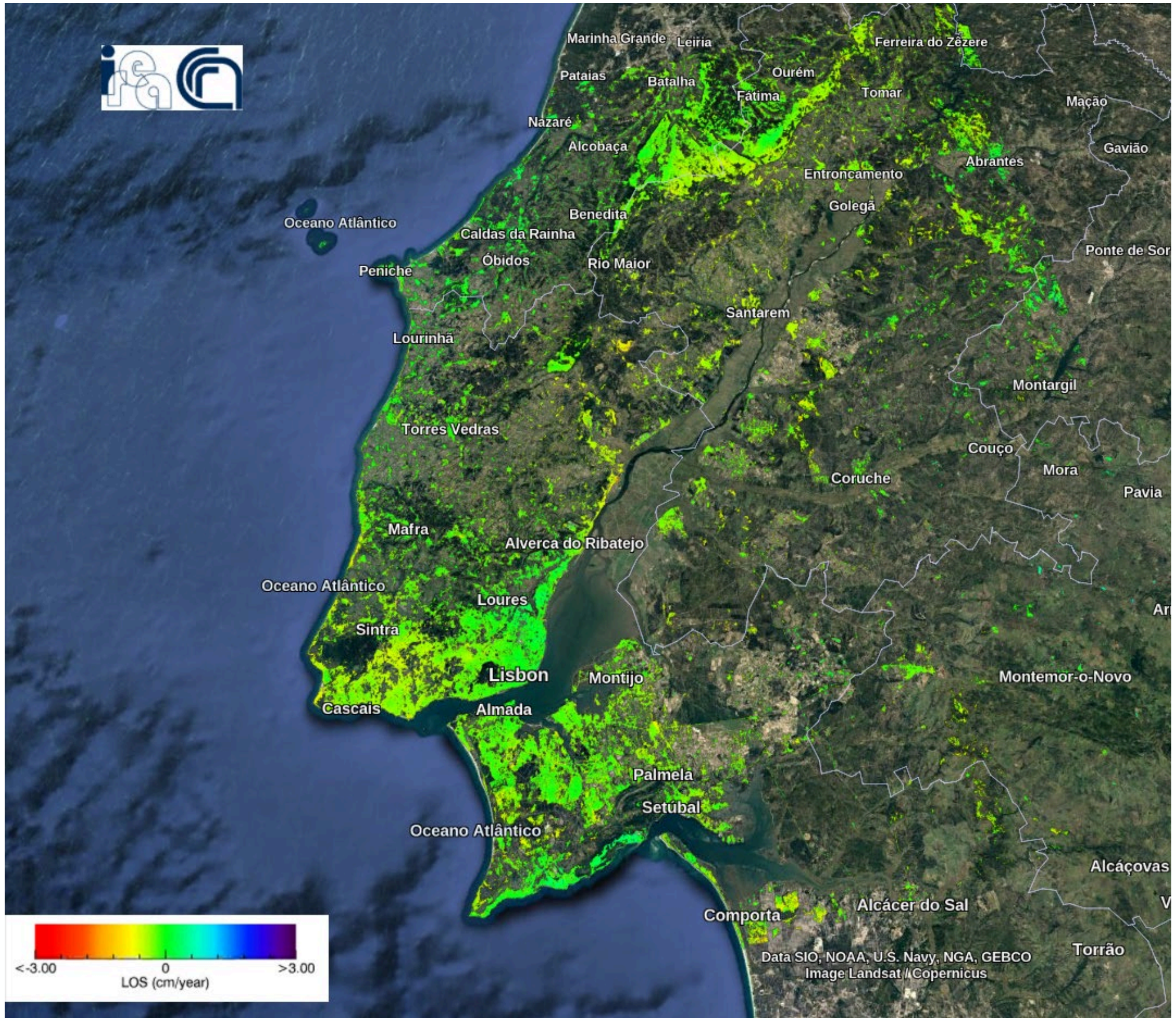

Start Date	26/01/2018
End Date	27/04/2020
Number of Images	50
DEM	SRTM1 arcsec
Temporal Coherence	0.6
Bounding Box	38.088 , -11.124 39.800 , -7.945
Orbit Direction	Ascending

The selected parameters using the P-SBAS service at G-TEP platform to create Lisbon deformation velocity map, the interferograms and the coherece map.

The Main Idea of The Methodology

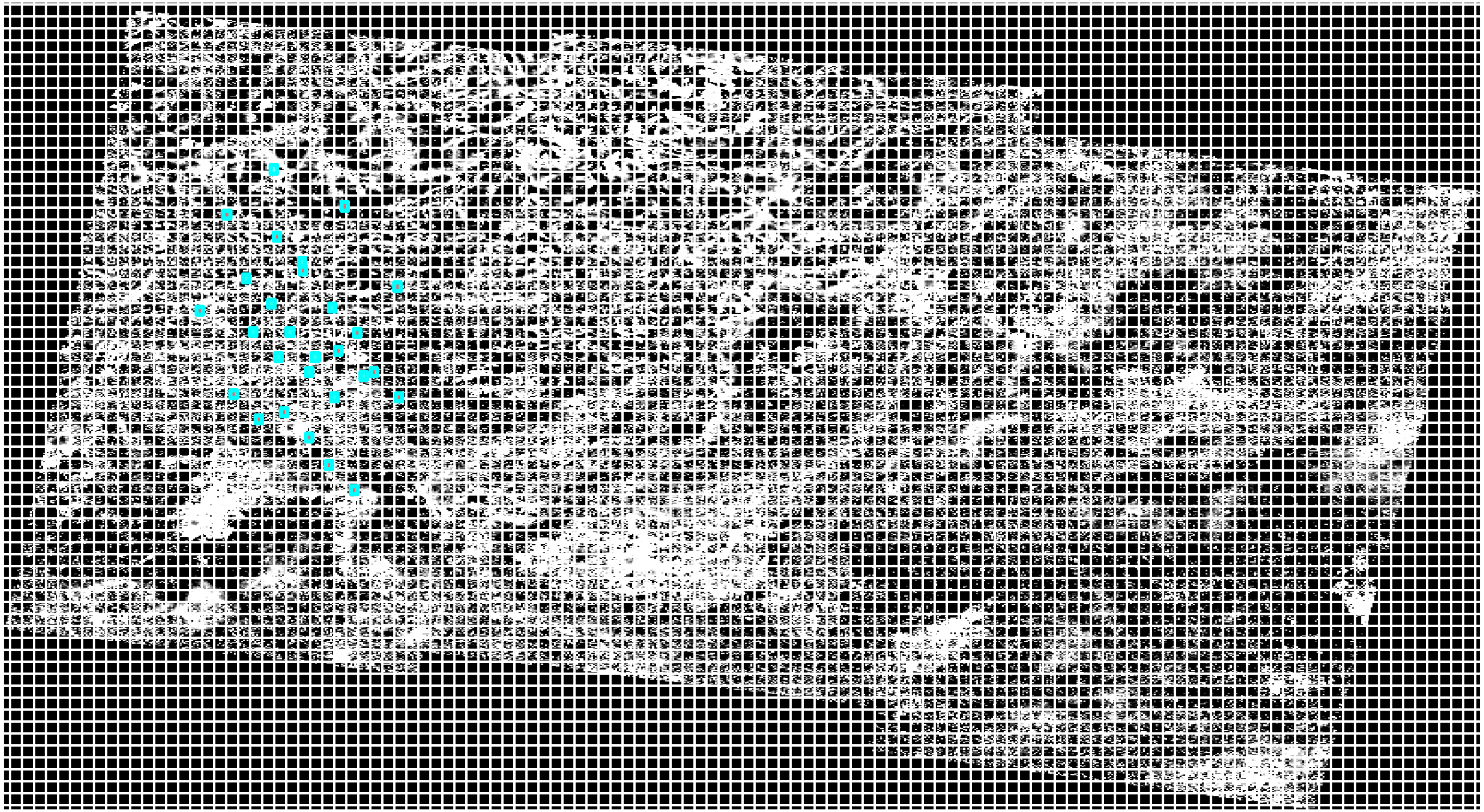

Measurement Point

The Main Idea of The Methodology

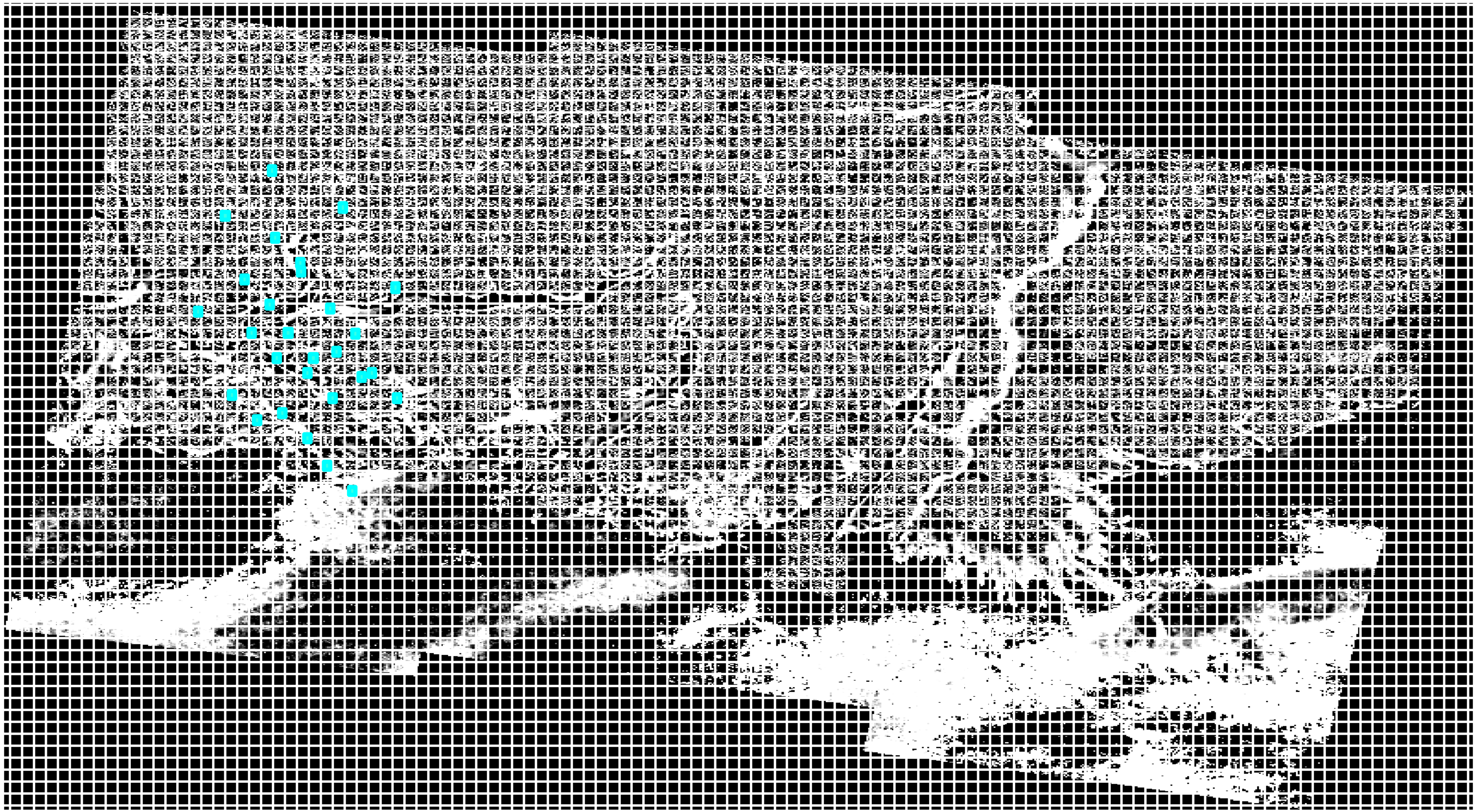

The Main Idea of The Methodology

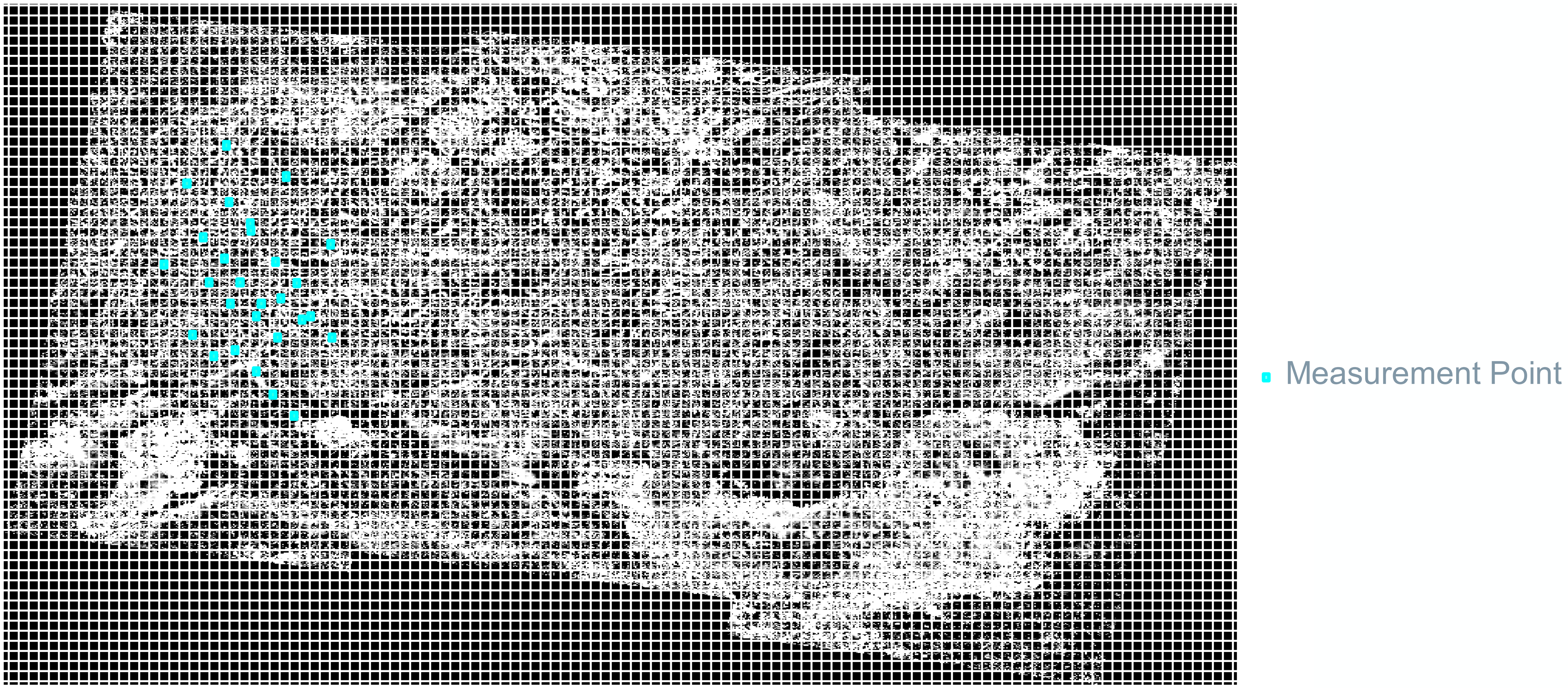

The Creation of The Datasets

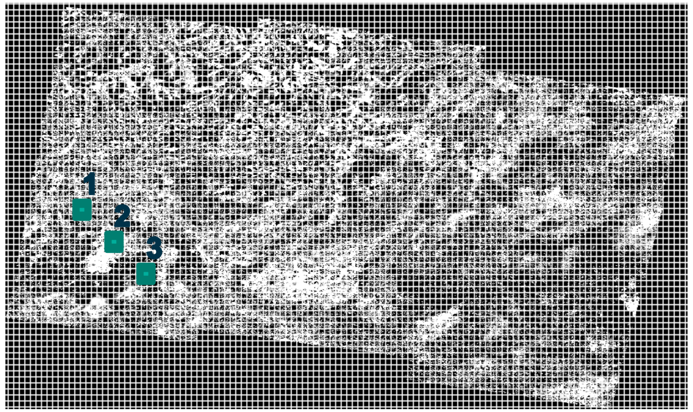

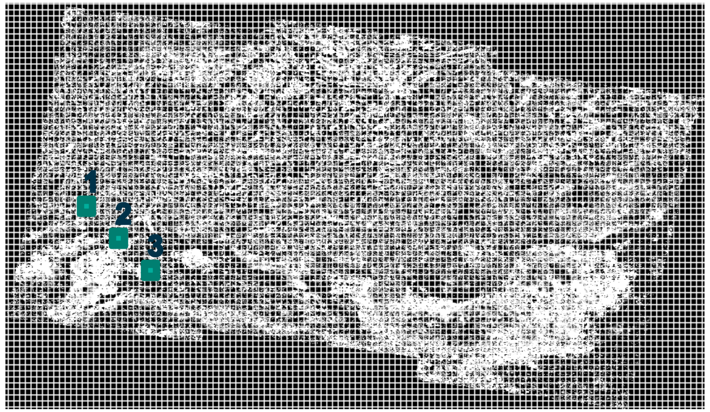

	1st Interferogram	2nd Interferogram	Last Interferogram	VEL	Label (0.7cm/year)
1	1.15	3.10	2.05	-1.5	Fast Negative / Negative / Undefined
2	-2.10	2.55	-3.09	0.9	Fast Positive / Positive / Undefined
3	-1.75	-1.15	-1.68	-0.1	Undefined / Negative

Training Examples
Phase Values (Radian)

Labels ??
The Velocity Values of The Measurement Point Inside The Pixel (cm/year)

The Sequence of The Wrapped Interferograms

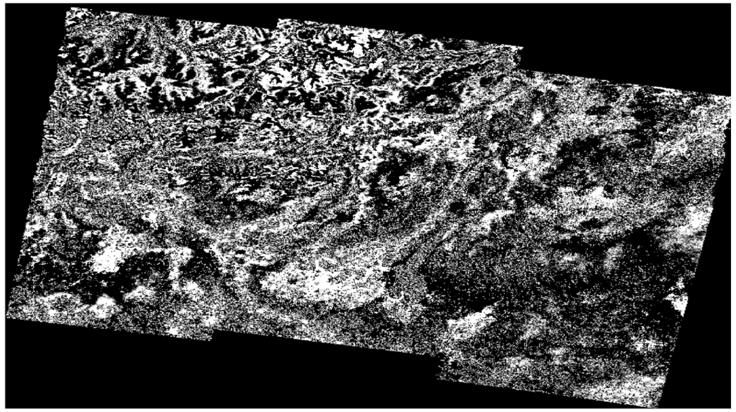

20191205 - 20191223

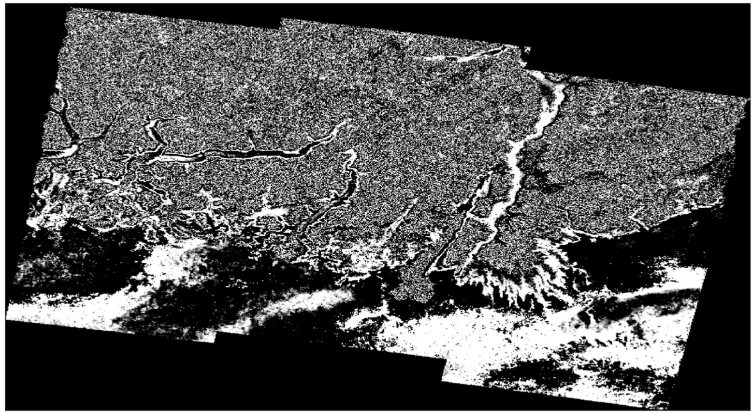

20200110 - 20200304

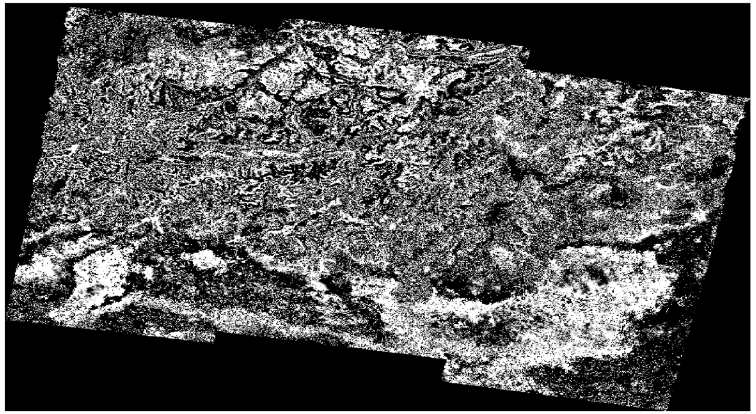

202000409 - 20200427

The generated interferograms by P-SBAS G-TEP were sorted chronologically before creating the dataset and inputting the training samples into the model

Sorting The Wrapped Interferograms Chronologically

The Sequence of The Temporal Baselines of The Interferograms

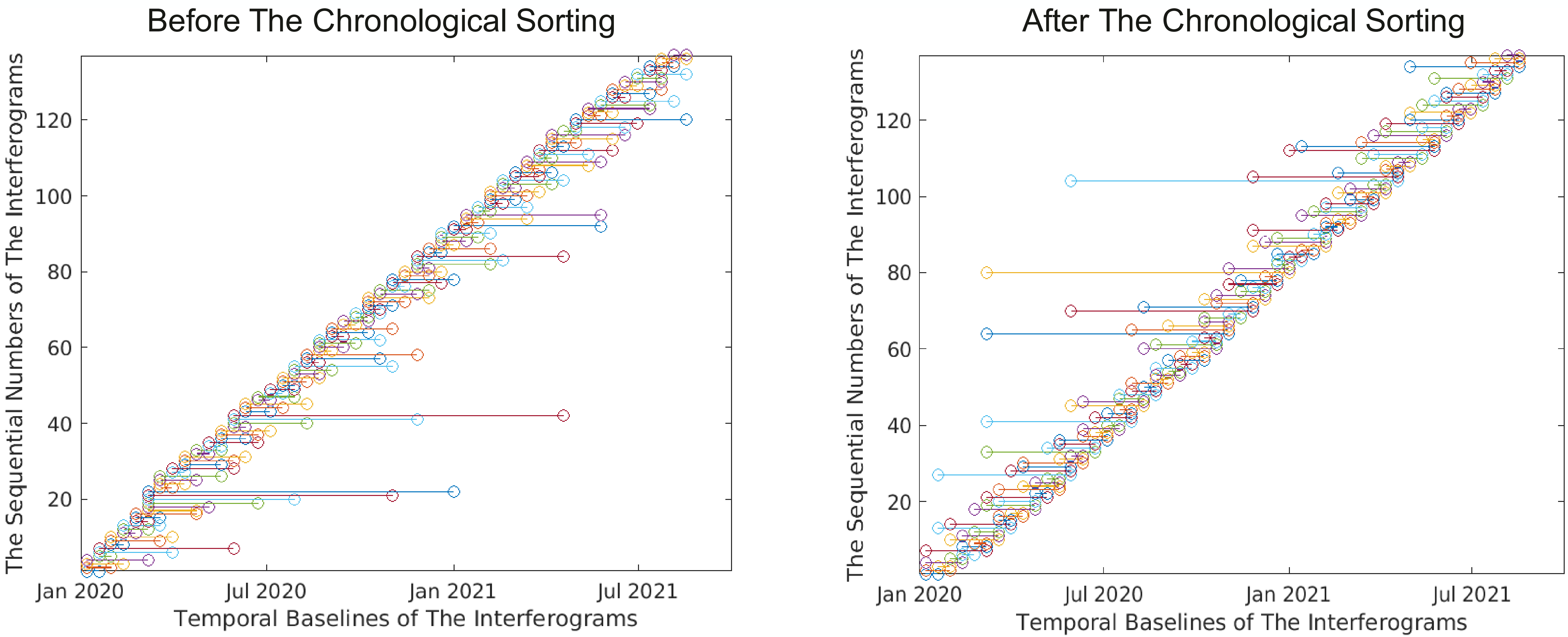

Sorting The Wrapped Interferograms Chronologically

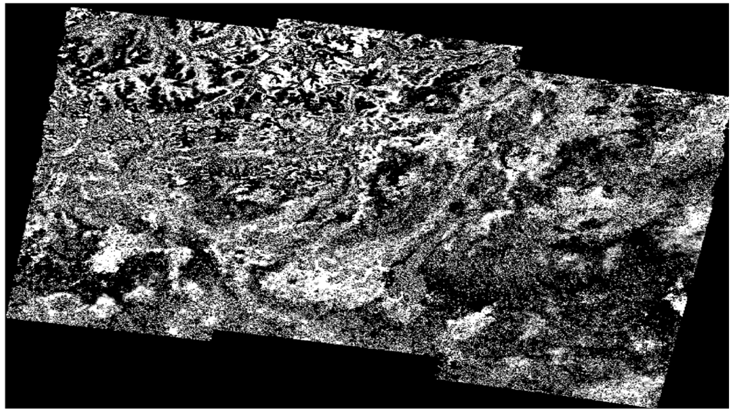

20191205 – 20191223 **(3)**

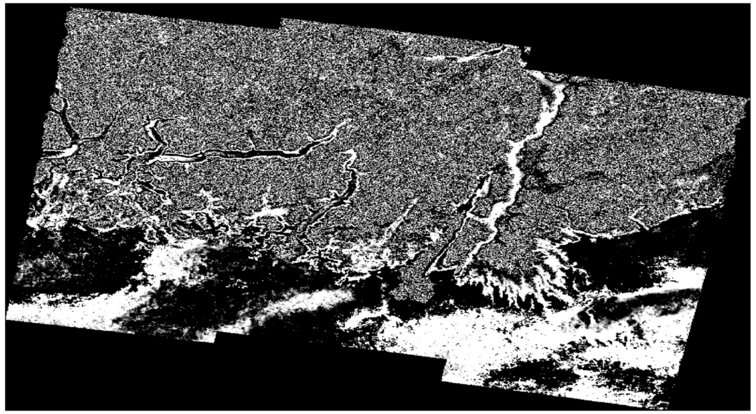

20200110 – 20200304 **(2)**

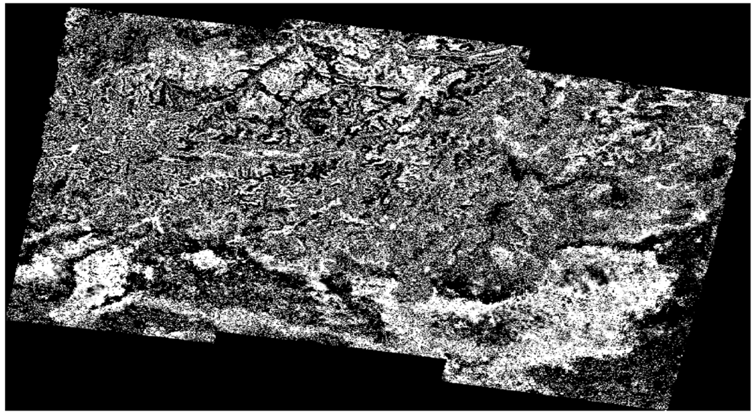

202000409 – 20200427 **(1)**

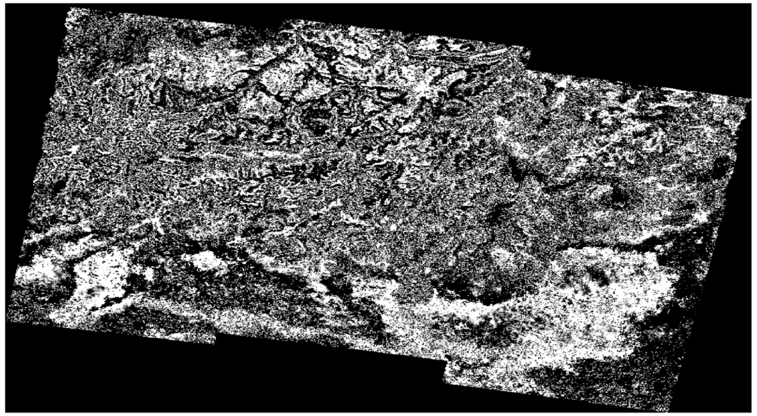

202000409 - 20200427

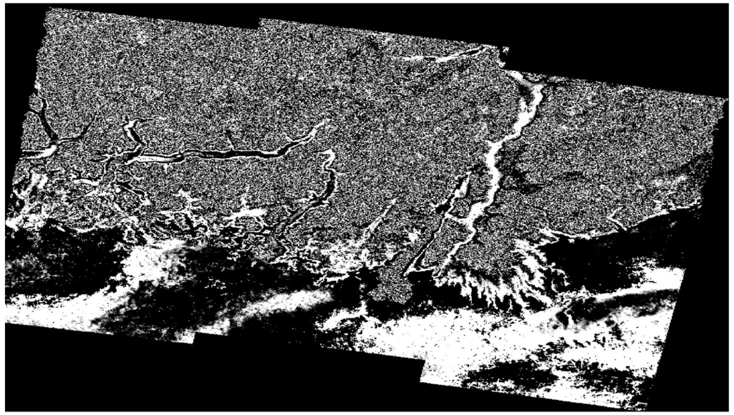

20200110 - 20200304

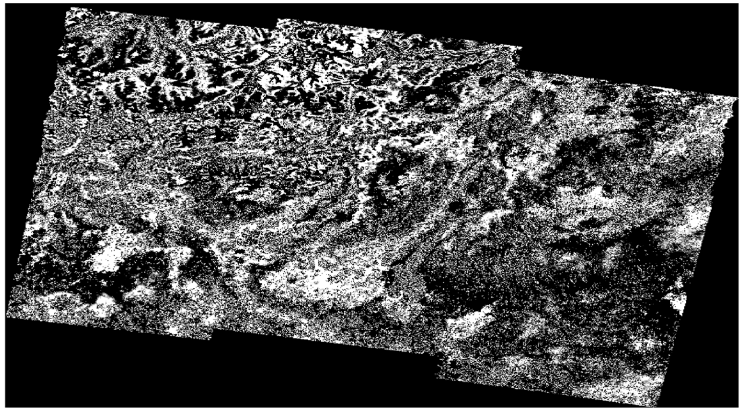

20191205 - 20191223

High-Pass Filtering

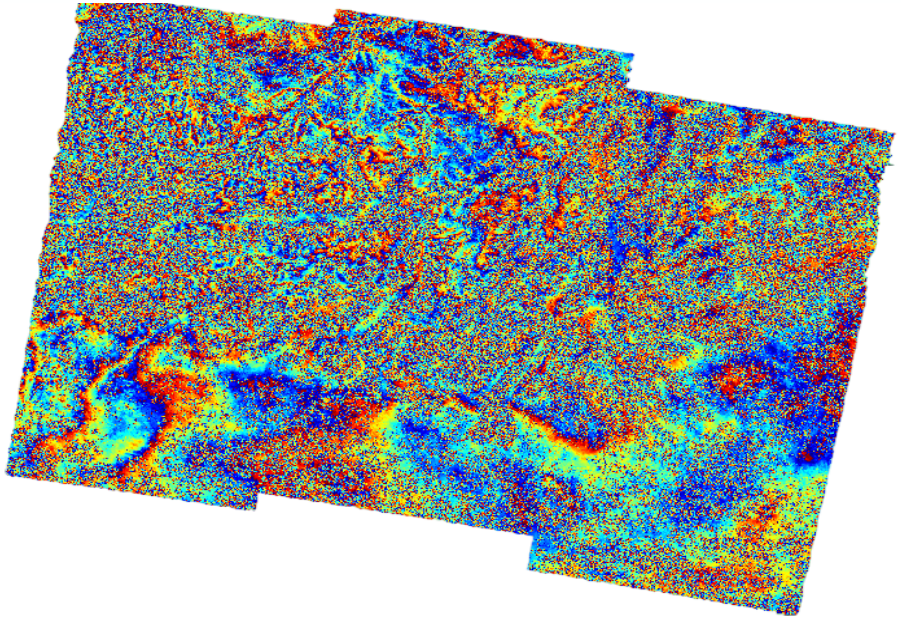

Wrapped Interferogram (Before Applying The High-Pass Filter)

- Considering that the main power of the low frequency signal comes from the atmospheric artifacts [6,7]

- By virtue of high pass filtering, the methodology effectively mitigates the highlighting of displacements sharing similar wavelengths

- As a result, The suitability of the methodology is enhanced for the precise detection and characterization of localized phenomena

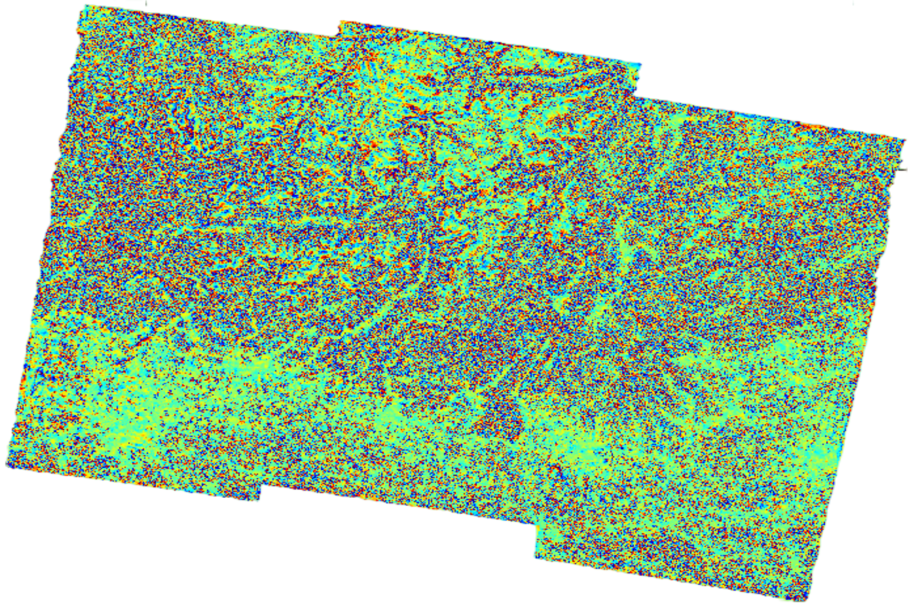

Wrapped Interferogram (After Applying The High-Pass Filter)

The Matrices Representing Slow and Fast Motion

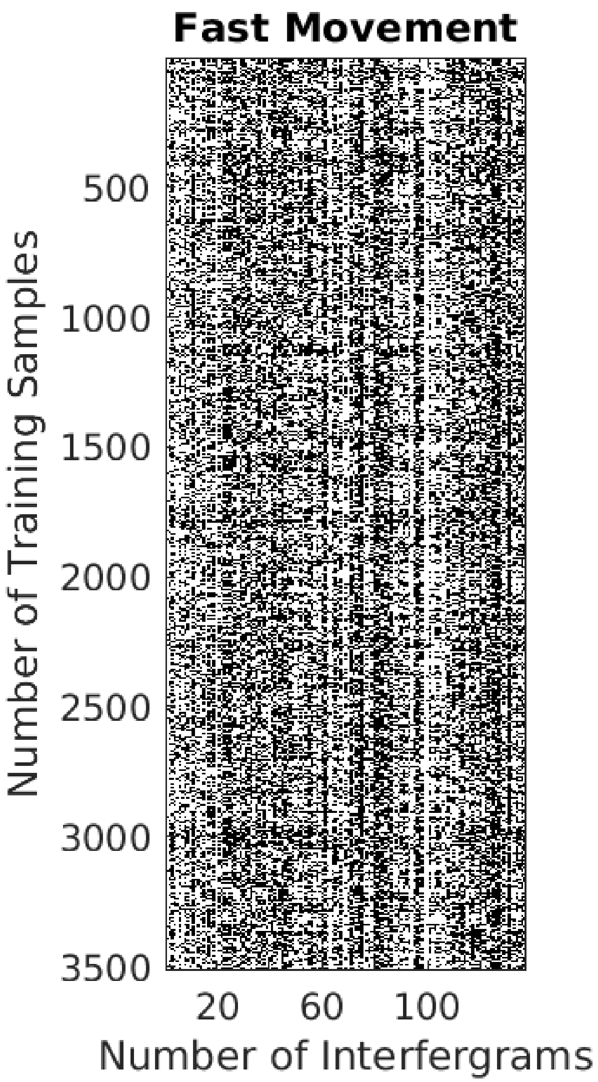

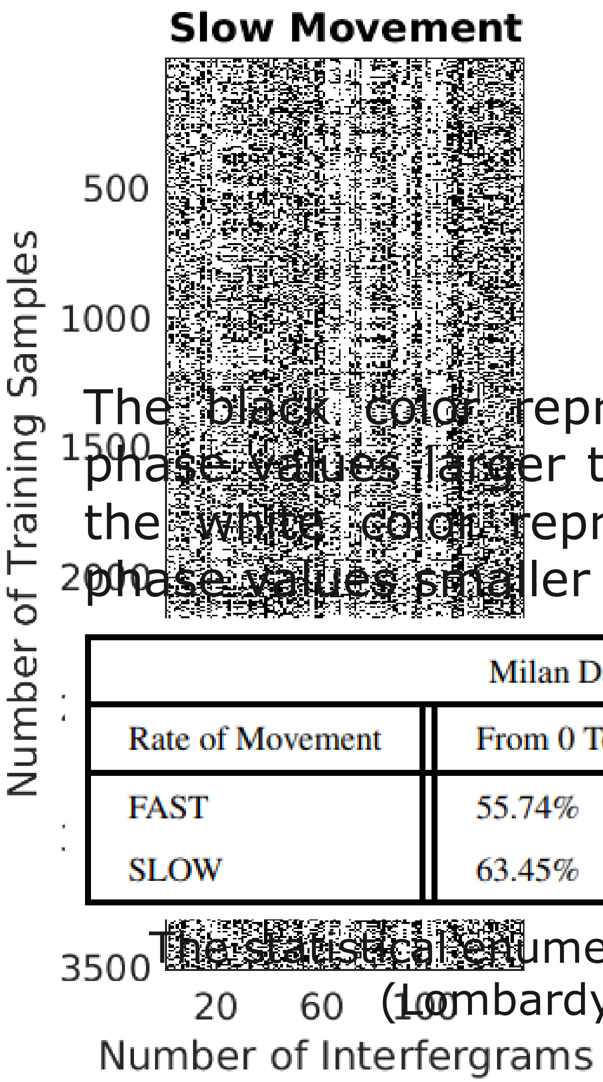

The black color represents the filtered phase values larger than 1 radian, while the white color represents the filtered phase values smaller than 1 radian

Milan Dataset		
Rate of Movement	From 0 To 1 Rad	From 1 To 2π Rad
FAST	55.74%	44.26%
SLOW	63.45%	36.55%

The statistical enumeration of data points (Lombardy Dataset)

The Matrices Representing Slow and Fast Motion

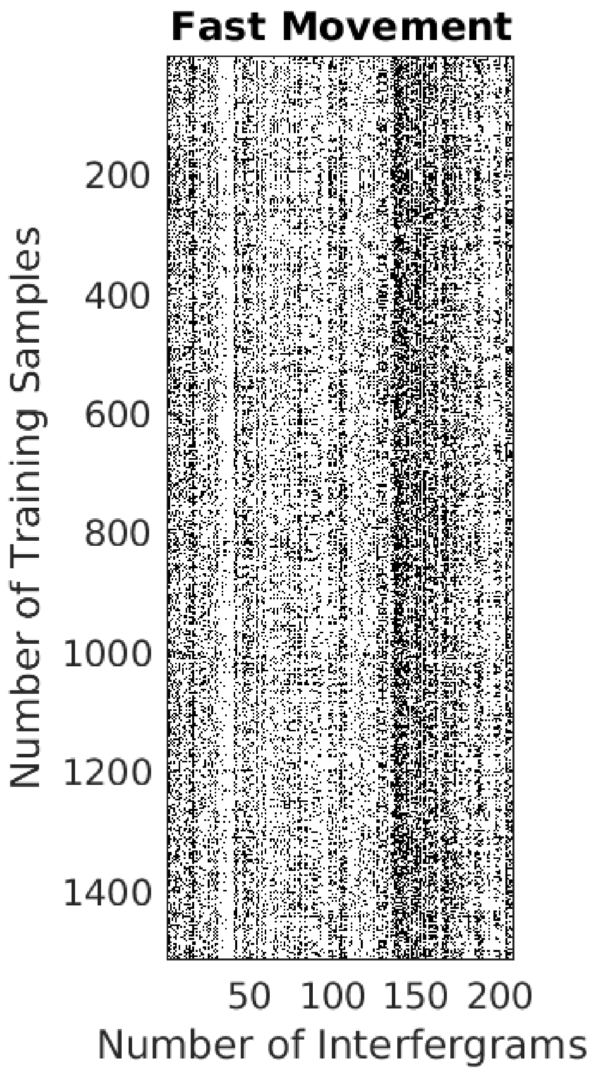

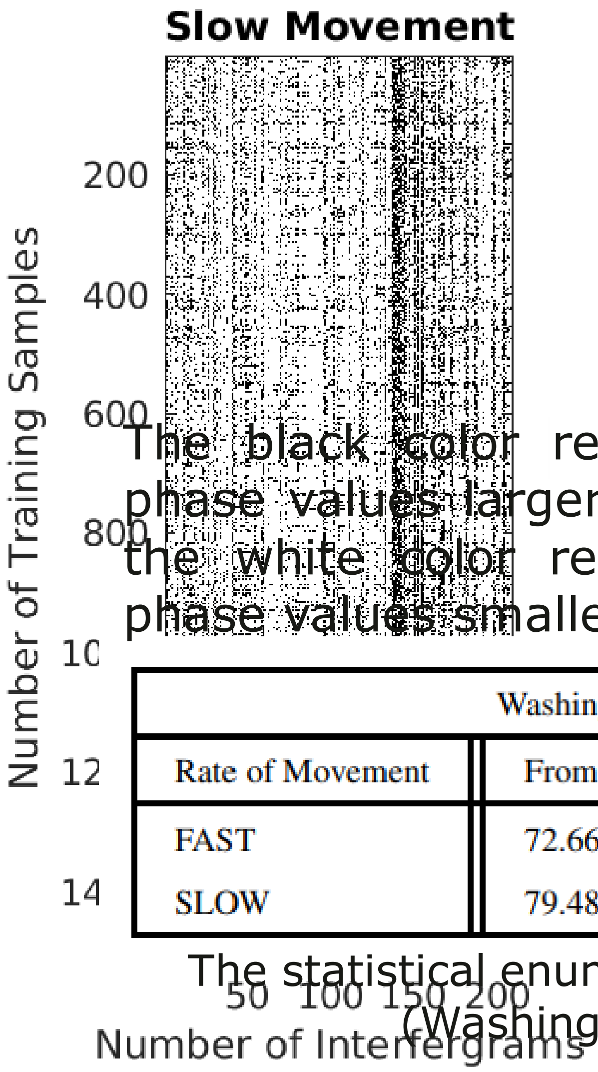

The black color represents the filtered phase values larger than 1 radian, while the white color represents the filtered phase values smaller than 1 radian

Washington Dataset		
Rate of Movement	From 0 To 1 Rad	From 1 To 2π Rad
FAST	72.66%	27.34%
SLOW	79.48%	20.52%

The statistical enumeration of data points (Washington Dataset)

The Matrices Representing Slow and Fast Motion

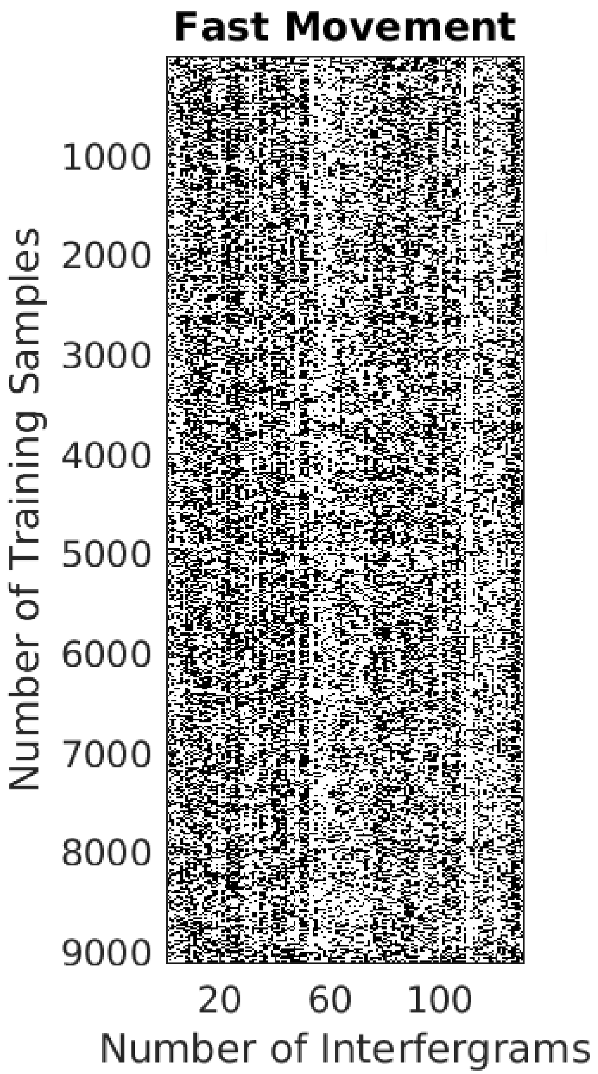

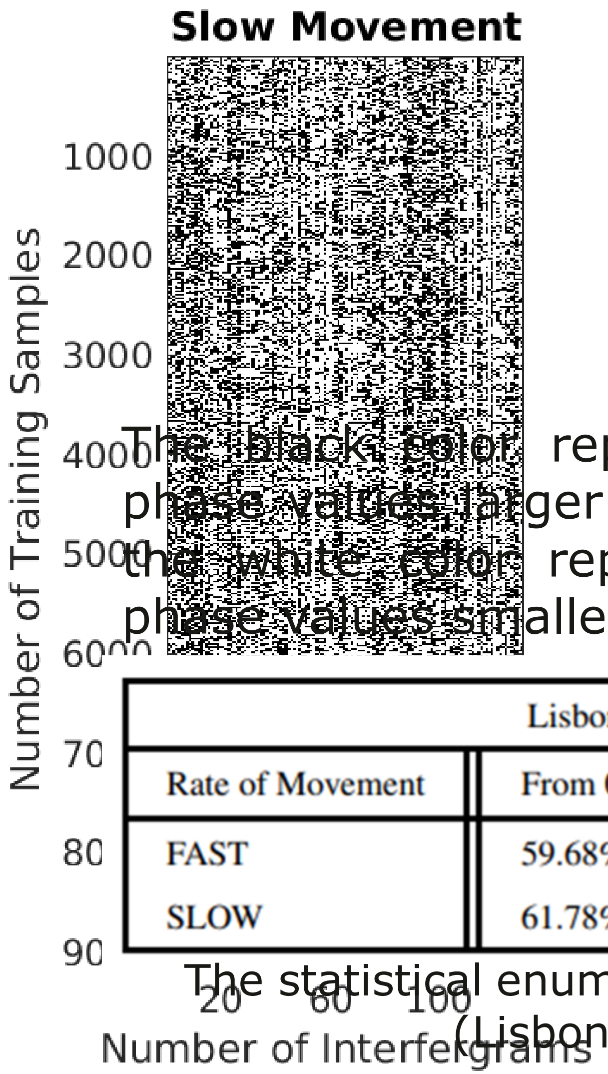

The black color represents the filtered phase values larger than 1 radian, while the white color represents the filtered phase values smaller than 1 radian

Lisbon Dataset		
Rate of Movement	From 0 To 1 Rad	From 1 To 2π Rad
FAST	59.68%	40.32%
SLOW	61.78%	38.22%

The statistical enumeration of data points (Lisbon Dataset)

The Best Three ML Methods for The Training

Results of the trained models*

Lisbon (Fast Positive/Undefined)	Washington (Fast Positive/Undefined)	Lombardy (Fast Positive/Undefined)
Subspace KNN (Ensemble) 83.7%	Cosine KNN 92%	Quadratic Discriminant 79.2%
Cubic SVM 83.7%	Cubic SVM 92%	Cubic SVM 77.7%
Cosine KNN 82.9%	Subspace KNN (Ensemble) 91.7%	Cosine KNN 74.3%
Lisbon (Fast Negative/Undefined)	**Washington (Fast Negative/Undefined)**	**Lombardy (Fast Negative/Undefined)**
Cosine KNN 82.5%	Subspace KNN (Ensemble) 87.2%	Cubic SVM 86.8%
Cubic SVM 81.4%	Cosine KNN 86.6%	Cosine KNN 86.2%
Quadratic Discriminant 80.5%	Cubic SVM 86.4%	Quadratic Discriminant 85.7%
Lisbon (Positive/Negative)	**Washington (Positive/Negative)**	**Lombardy (Positive/Negative)**
Cosine KNN 79.7%	Cosine KNN 76.4%	Cosine KNN 95.1%
Quadratic Discriminant 79.3%	Quadratic Discriminant 76%	Cubic SVM 94.9%
Bagged Tree (Ensemble) 77.6%	Cubic SVM 75.6%	Logestic Regression 94.4%

*Other experienced methods : Medium Neural Network, Medium Tree, Fine Tree, 2D Convolution Neural Network, and Long short-term memory

Comparison Between Cubic SVM and Cosine K-NN

Cubic SVM Model

- **Complexity**: High complexity
- **Number of Parameters**: Several parameters to tune
- **Implementation Field**: Suited for non-linear classification problems
- **Cost of Calculation**: High computational cost, both in terms of memory and CPU
- **Time of Training**: High

Cosine K-NN Model

- **Complexity**: Low to moderate complexity
- **Number of Parameters:** Few parameters to tune
- **Implementation Field:** Often used in text classification, document retrieval, and recommendation systems.
- **Cost of Calculation:** Moderate computational cost during inference, however, memory cost can be high because all training data must be stored
- **Time of Training:** Minimal to low

Psuedo-Labelling

A model is trained and tested on the labeled data

The trained model is used to make predictions on the psuedo-labelled data

A new training set is created by combining the testing samples with a prediction accuracy of 0.9 or higher with the original labeled data

The pseudo-labeled training samples are removed from the original test set of unlabeled training samples

The model is retrained using the combined labeled and pseudo-labeled data

Psuedo-Labelling Results

	Cosine K-NN	1st PS	2nd PS
Number of training samples	1108	1712	4668
Number of testing samples	276	428	10890
Accuracy of validation	75.5%	83.7%	97.5%
Accuracy of the test set	74.3%	85.8%	97.4%

Results of Pseudo-Labelling PS on Lombardy Dataset (Fast Positive/Undefined)

	Cosine K-NN	1st PS	2nd PS	3rd PS
Number of training samples	4884	5928	6718	2792
Number of testing samples	1220	1482	1680	6512
Accuracy of validation	85.6%	87.5%	89.7%	89.8%
Accuracy of the test set	86.6%	89.6%	90%	89.9%

Results of Pseudo-Labelling PS on Washington Dataset (Fast Negative/Undefined)

	Cosine K-NN	1st PS	2nd PS	3rd PS
Number of training samples	14596	17460	18988	20196
Number of testing samples	3650	4366	4748	5050
Accuracy of validation	79.7%	83.1%	84.8%	85.7%
Accuracy of the test set	79.7%	83%	84.7%	85.3%

Results of Pseudo-Labelling PS on Lisbon Dataset (Positive/Negative)

Psuedo-Labelling Results

Fast Positive-Undefined Movement Classification

True Class \ Predicted Class	Fast Positive	Undefined
Fast Positive	5321	124
Undefined	162	5283
	97.0%	97.7%
	3.0%	2.3%

Lombardy Dataset

Fast Negative-Undefined Movement Classification

True Class \ Predicted Class	Fast Negative	Undefined
Fast Negative	2965	291
Undefined	370	2886
	88.9%	90.8%
	11.1%	9.2%

Washington Dataset

Positive-Negative Movement Classification

True Class \ Predicted Class	Negative	Positive
Negative	2189	379
Positive	369	2199
	85.6%	85.3%
	14.4%	14.7%

Lisbon Dataset

Confusion Matrices for The Trained Models

The Ground-t e Predictions

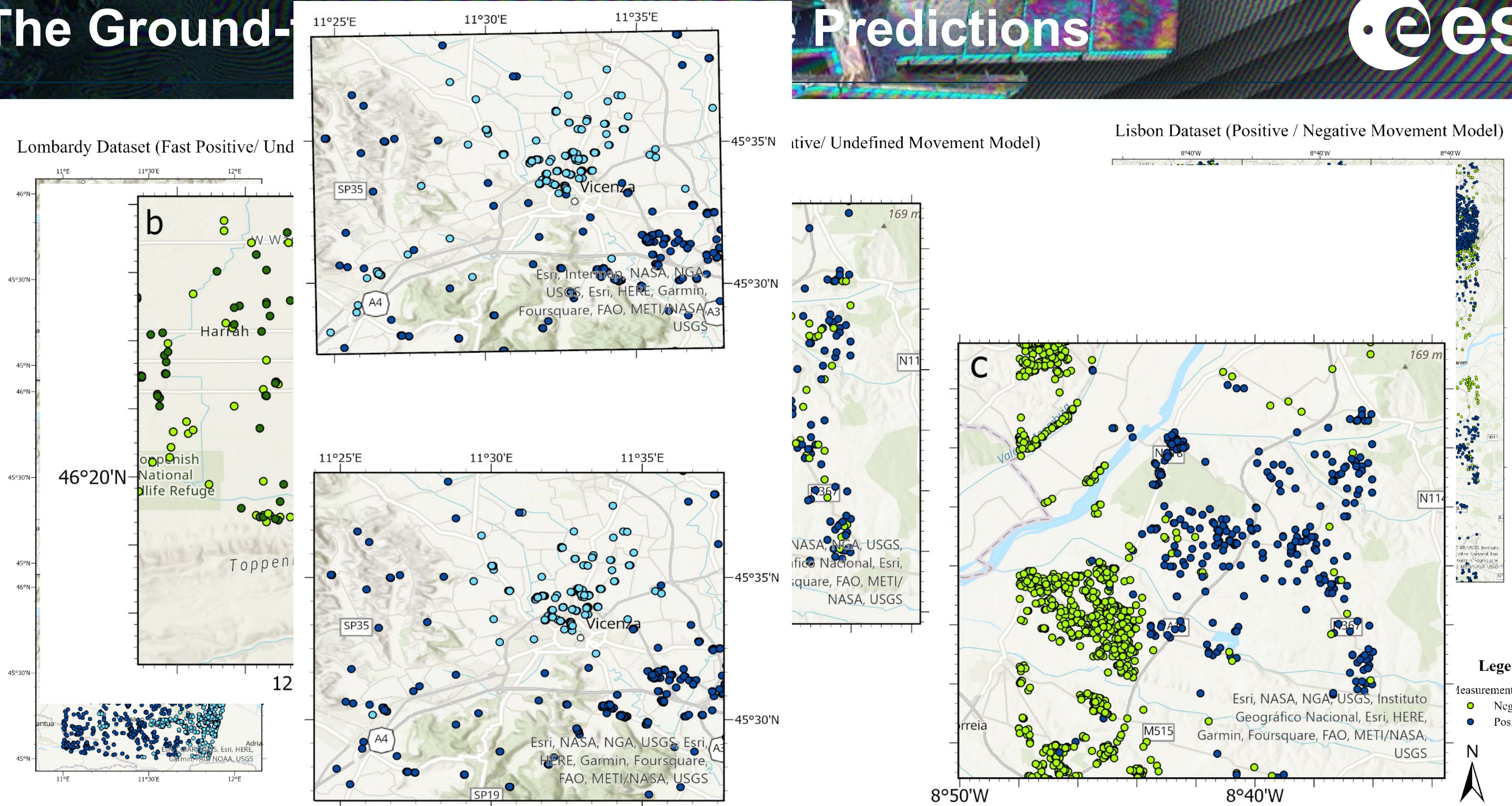

Figure A displays the training dataset. Figure B displays the ground truth of the test dataset. Figure C displays the predictions of the test dataset.

Masked Roads Network

Fast Positive Roads Movement Indication (Lombardy Dataset)

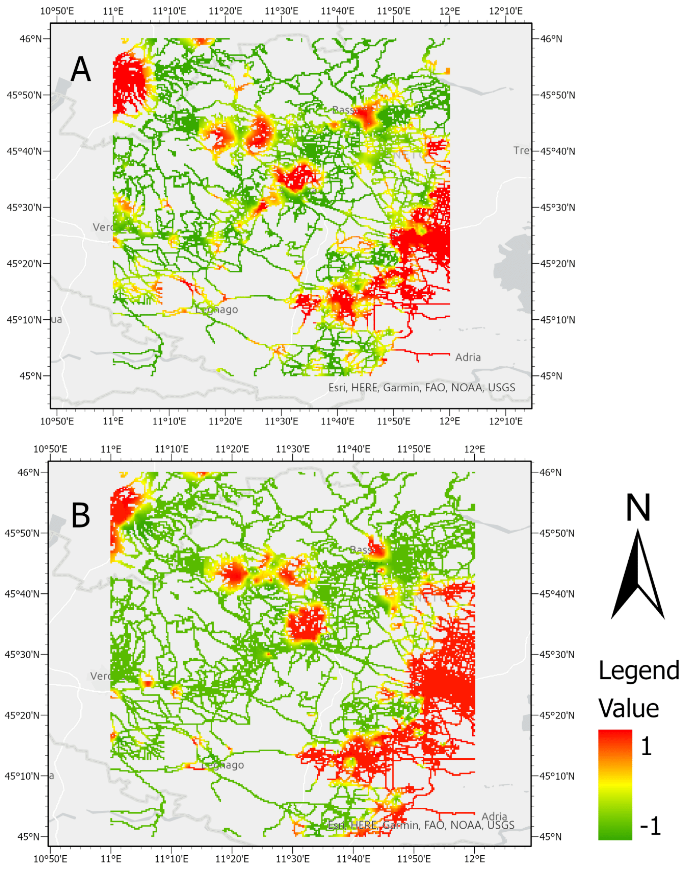

High Negative Roads Movement Indication (Washington Dataset)

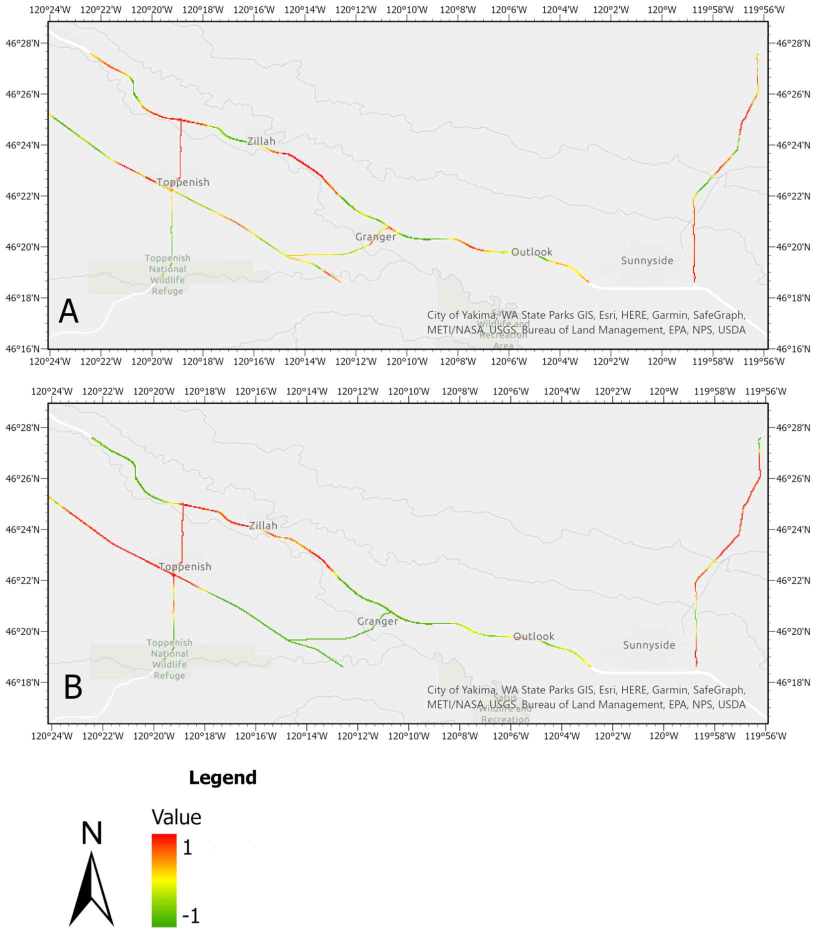

Positive/Negative Roads Movement Indication (Lisbon Dataset)

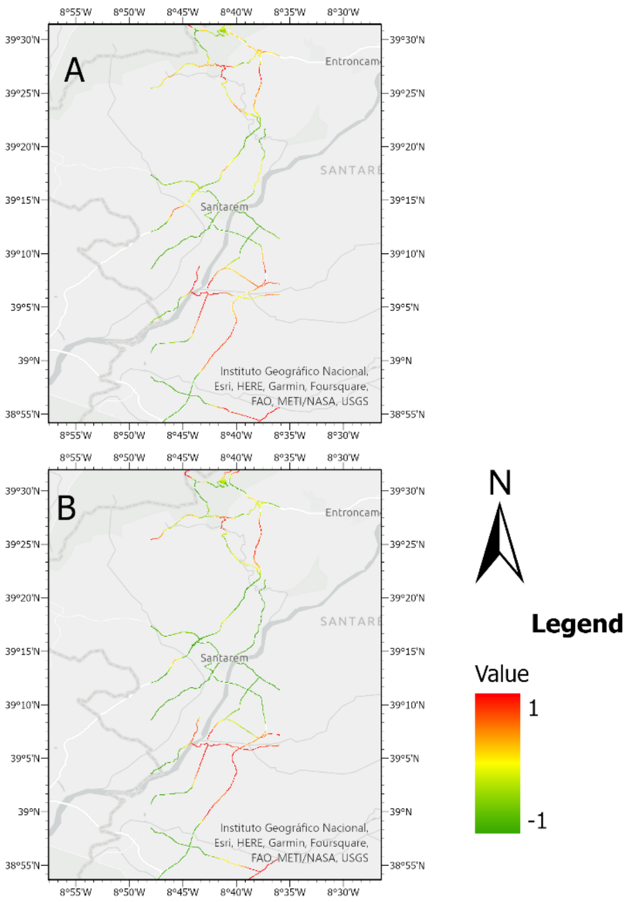

Conclusion

- ✓ Artificial intelligence, particularly Machine Learning, is effective for extracting deformation signals from the developed datasets
- ✓ A number of Machine Learning methods were tested, and Cosine K-NN showed the highest suitability for detecting the class of moving pixel, especially in adjacent regions
- ✓ To address low validation accuracy, pseudo-labeling was employed, leading to significant improvements
- ✓ The trained models worked consistently across three different geographical datasets, although further validation is needed
- ✓ Main roads networks were masked to predict their movement sensitivity
- ✓ Testing the Persistent Scatterer Interferometry technique using this workflow for further evaluation is recommended

REFRENCES

1. Crosetto, M., Castillo, M., & Arbiol, R. (2003). Urban subsidence monitoring using radar interferometry. *Photogrammetric Engineering & remote sensing*, *69*(7), 775-783.
2. He, L., Wu, L., Liu, S., Wang, Z., Su, C., & Liu, S. N. (2015). Mapping two-dimensional deformation field time-series of large slope by coupling DInSAR-SBAS with MAI-SBAS. *Remote Sensing*, *7*(9), 12440-12458.
3. J. Jung, D.-j. Kim, and S.-E. Park, "Correction of atmospheric phase screen in time series insar using wrf model for monitoring volcanic activities," IEEE Transactions on Geoscience and Remote Sensing, vol. 52, no. 5, pp. 2678– 2689, 2013.
4. Vijayan, M. S., & Mohan, M. A. (2015). Contourlet based edge enhancement and detection in SAR images. *IJERT*, *4*(5), 1079-1083.
5. X. Li, F. Zhang, Y. Li, Q. Guo, Y. Wan, X. Bu, Y. Liu, and X. Liang, "An elevation ambiguity resolution method based on segmentation and reorganization of tomosar point cloud in 3d mountain reconstruction," Remote Sensing, vol. 13, no. 24, p. 5118, 2021.
6. Siddique, M. A., Wegmuller, U., Hajnsek, I. and Frey, O., 2018. ¨ Sar tomography as an add-on to psi: Detection of coherent scatterers in the presence of phase instabilities. Remote Sensing 10(7), pp. 1014.
7. Rhodes, R. H., Fa¨ın, X., Brook, E. J., McConnell, J. R., Maselli, O. J., Sigl, M., Edwards, J., Buizert, C., Blunier, T., Chappellaz, J. et al., 2016. Local artifacts in ice core methane records caused by layered bubble trapping and in situ production: a multi-site investigation. Climate of the Past 12(4), pp. 1061–1077.

THANK YOU